JOURNAL OF CATALYSIS 148, 164–180 (1994)

On the Interaction of 1-Propanamine with Cation-Containing MFI Zeolite

Vladislav I. Kanazirev,[1] Geoffrey L. Price, and Kerry M. Dooley

Department of Chemical Engineering, Louisiana State University, Baton Rouge, Louisiana 70803

Received November 3, 1993; revised February 11, 1994

The interaction of 1-propanamine (1-PA) with H–MFI zeolite and its Ga, In, and Cu modifications, prepared by solid state ion exchange, has been studied by thermal analysis, high resolution gas chromatography, mass spectrometry, and catalytic reactor experiments. Two completely different desorption features have been observed when the H–MFI sample is first equilibrated with 1-PA at 323 and 593 K and then heated to 823 K. These desorption features have been ascribed to the decomposition of propylammonium and dipropylammonium ions adsorbed at the proton sites of the zeolite. Catalytic experiments confirmed dipropylamine as the major product of 1-PA conversion at 593 K over an H–MFI catalyst. In contrast, a radical change in the interaction of 1-PA with the zeolite has been observed as a result of the replacement of the protons in MFI with Ga, In, or Cu cations. More than one 1-PA molecule can be coordinated to a cation even at relatively high temperatures, facilitating both bimolecular transalkylation and dehydrogenation processes. The desorption features of 1-PA with cation containing MFI differ generally from those of pure H–MFI zeolite. NH_3 product is desorbed at temperatures as much as 160 K below that of H–MFI. Nitriles, C_2–C_6 hydrocarbons, and some aromatics appear in appeciable amounts in the decomposition products. Gas-phase hydrogen inhibits the dehydrogenation processes and prevents the formation of a residue.

Catalytic experiments in a gradientless batch recirculating reactor have revealed that different dehydrogenation reactions predominate depending on the nature of the zeolite cation. While a C_6-imine appears as a major product of the reaction of 1-PA over In–MFI, more dehydrogenated N-containing compounds such as propionitrile and a C_6-nitrile predominate over Ga–MFI and Cu–MFI, respectively. These differences can be interpreted in terms of the differing Lewis acid strengths and reducibilities of the Ga, In, and Cu cations.

INTRODUCTION

Nitrogen-containing organic compounds have been used in the synthesis of zeolites since the earliest efforts (1, 2). A number of zeolite structures such as MFI, offretite, β-zeolite, and aluminophosphates can be produced using amines as organic templates (3–5). The decomposition of the organic template, often by thermal treatment in air, is well recognized as a crucial step in obtaining quality adsorbents or catalysts, so this process has been studied intensively.

Early work on the decomposition of alkylamines in zeolites was concentrated on offretite and other zeolites which retained alkylamines during the crystallization process. Wu *et al.* (6) investigated the decomposition of tetramethylammonium offretite and observed a very complex product. Twenty-one low molecular weight products including methanol, CO, C_2–C_4 alkenes, and H_2 were detected by mass spectrometry (MS) and IR, along with traces of acetylenes and N-containing compounds. More detailed studies have been performed on Y-type zeolite exchanged with organic cations (7–9). Although studies were directed at determining the mechanism of formation of acidic centers, valuable information about the decomposition pathways of alkylammonium cations has also been obtained. Deamination of primary alkylammonium-containing zeolites was found to produce a stoichiometric hydrogen Y zeolite, but considerable dehydroxylation was observed in the case of samples which contained secondary and tertiary alkylammonium ions (8). Jacobs and Uytterhoeven suggested that at elevated temperatures Hofmann elimination of the alkylammonium ion takes place. At lower temperatures, the appearance of $(CH_3)_3N$ and CH_3NH_2 among the products of decomposition of a dimethylammonium zeolite Y was explained by the authors as a transalkylation process

$$2[(CH_3)_2NH_2^+Z^-] \rightarrow CH_3NH_3^+Z^- + (CH_3)_3NH^+Z^-, \quad [1]$$

where Z^- is the anionic zeolite framework.

The advent of high-silica zeolites has stimulated further research on the decomposition of alkylamine templates. Most high-silica zeolites are synthesized in the presence of quaternary ammonium cations or amines that decompose upon thermal treatment resulting in a partly protonated zeolite (3). Parker *et al.* (10) studied the decomposition of a tetraethylammonium MFI zeolite and concluded that

[1] On leave from the Bulgarian Academy of Sciences, Institute of Organic Chemistry.

0021-9517/94 $6.00

tetraalkylammonium ions are associated with the strong acid sites of the zeolite. Recently, the coupling of thermal analysis (TA) with high resolution gas chromatography (GC) and mass spectrometry (MS) has been shown to be an effective technique for the characterization of the volatile products resulting from the thermal decomposition of tetra-, tri-, di-, and monopropylammonium cations occluded in MFI zeolites (11, 12). Propene was observed as the major product, which suggests a decomposition mechanism similar to Hofmann elimination. Several side reactions including oligomerization, cyclization, and hydrogen transfer appear to be responsible for the complex composition of the volatile products, which includes aromatic hydrocarbons and long chain alkanes (11, 12). Catalytic effects on secondary reactions are more pronounced when framework B, Fe, or Ga are present, but nitrogen-containing compounds other than amines have not been observed in the volatile products (11).

The thermal decomposition of tetraethylammonium (TEA) in zeolite beta has been studied in air and argon using a combined TA–MS technique (13). Sequential Hofmann elimination reactions have been confirmed as the main decomposition route of the organic template. Furthermore, the re-adsorption of ethylene and light alkylamines at acid sites led to the formation of a residue. The desorption of strongly basic decomposition products, including ammonia, required temperatures as high as 773 K.

In a series of publications (14–17) Gorte and co-workers advanced an interesting approach for the determination of the proton acidity of high-silica zeolites that is based on the peculiarities of the interaction of amines and other simple organic molecules with zeolitic protons. The authors showed the existence of stoichiometric 1–1 proton–amine complexes, particularly for propanamines interacting with Brønsted acid centers of H–MFI, isomorphously substituted MFI, and aluminophosphates. The simultaneous evolution of propene and ammonia during the thermal decomposition of the complexes was observed and could be used for the purpose of counting the proton acid sites of the samples investigated; these observations are similar to the earlier work of Jacobs and Uytterhoeven (8). In recent work of Gorte's group (18), the addition of Cu^{2+} to H–MFI led to significant changes in the TPD of 2-propanamine. The appearance of a new high temperature decomposition feature was ascribed to a Cu–amine interaction.

Despite the extensive work on both alkylamine decomposition and adsorption on zeolites, important aspects may have been overlooked. Such aspects include nitrile or HCN formation (19–22), oligomerizations, especially at low amine pressures (23–25), and disproportionation reactions (22, 26). Recently, Tanabe and co-workers reported that the decomposition of alkylamines can be directed exclusively to a selective dehydrogenation leading to nitriles; they used weakly basic oxides such as ZrO_2 or hybrid acid–base catalysts (26, 27).

It is clear that alkylamines can react according to different pathways depending upon the catalyst and reaction conditions. Moreover, alkylamines are highly basic and can be strongly held by acidic zeolites. While simple unimolecular decomposition of adsorbed alkylamines to an alkene and ammonia (Hofmann elimination) appears to be the sole reaction at low amine coverages over purely H-forms of high-silica zeolites, a few literature references (e.g., (6)) point to the possibility of forming traces of unsaturated N-containing products (nitriles, HCN) during the decomposition of the organic template in other zeolites.

Recently, we applied the approach developed by Gorte and co-workers (14–17) for the characterization of the acid properties of Ga-modified MFI zeolites. There were numerous indications that the presence of Ga cations resulted in a mode of propanamine adsorption and subsequent reaction upon temperature programming that deviated from the Hofmann elimination route. The purpose here is to describe this chemistry for MFI zeolites containing Ga, In, and Cu cations. We have used a microbalance, flow and batch recirculating reactors coupled with MS and GC for product characterization. We show that the presence of certain cations in the MFI zeolite radically alters the reaction pathways of propanamines compared to the corresponding H-zeolite. The nature of the residue produced during propanamine decomposition, and the important role of hydrogen in the thermal analysis and catalytic experiments, will be also discussed.

EXPERIMENTAL

Catalyst materials were prepared by intimate mechanical mixing of a host H–MFI zeolite (UOP MFI, 40/1 SiO_2/Al_2O_3, 10.5% water, completely protonated) with a metal oxide. Ga_2O_3 (Ingal Co.), In_2O_3 (American Smelting), and CuO (Aldrich) were the metal-containing reagents. The oxides and H–MFI were ball-milled for 3 h at a loading equivalent to one metal atom per framework aluminum atom, except for a single material which contained half the gallium (1 Ga/2 Al). This material will be specially highlighted where appropriate. We refer to the 1/1 *Me*/Al (*Me* = Ga, In, or Cu) materials as Ga–MFI, In–MFI, and Cu–MFI. Only one other material was prepared, a gallium-containing H–MFI via incipient wetness impregnation of $Ga(NO_3)_3$ on the H–MFI base at a loading of 1/1 Ga–Al which we refer to as Ga–MFI(imp); the method is reported elsewhere (28). This material was used in the batch catalytic reactor experiments and has shown activity and properties which are very similar to Ga–MFI. Catalysts were pelletized, crushed, and sieved to 0.4-0.8 mm particles prior to use.

Microbalance TA experiments were performed on a Perkin–Elmer TGA7 interfaced to a PC and utilizing a versatile gas and adsorbate supply system. Ten to fifteen mg of catalyst was placed on the Pt microbalance pan. A 50 cm^3/min He stream continuously purged the microbalance mechanism and mixed with a reagent gas stream prior to flow over the sample. The reagent gas total flow was also 50 cm^3/min of either pure He or a reducing mixture of 25 cm^3/min H_2 and 25 cm^3/min He so that the total flow was 100 cm^3/min sweeping the catalyst. The reagent gas mixture could also be diverted through a room temperature bubbler which nearly saturated the reagent gas stream with adsorbate. 1-Propanamine (1-Pa) and dipropylamine (DPA; 1-propanamine, *N*-propyl) adsorbates were used in this study.

Ga–MFI and In–MFI for microbalance TA experiments were first dried in the microbalance in pure He flow by temperature programming from 298 to 848 K at 166.7 K/ks (10 K/min) and a final hold at 848 K for 1.8 ks. Cu–MFI was subjected to a similar treatment but the final temperature was 973 K for 10.8 ks. To form "reduced" catalysts, the samples were further treated with the H_2-containing reagent gas for 10.8 ks at 848 K (gallium materials) or 10.8 ks at 623 K (indium materials). Cu–MFI was not subjected to H_2 reduction.

Propanamine TA experiments began by first cooling the material rapidly from the drying or reduction temperature to the adsorption temperature which was usually 323 K, although 423 and 593 K adsorption temperatures were sometimes used. The reagent gas stream was then diverted through the bubbler and adsorption continued for 0.3 ks. The bubbler was then bypassed and the sample was purged at the adsorption temperature for 0.6 ks. Thermal analysis was then accomplished by linear temperature programming from the adsorption temperature to 823 K at 83.3 K/ks (5 K/min).

Parallel TA experiments were also performed using a flow reactor apparatus with an MS detection system, described previously (28, 29). Conditions were identical to those of the microbalance experiments wherever possible, but 50 mg of catalyst, placed between two quartz wool plugs, was used. After pretreatment, the catalyst was cooled quickly to 323 K and evacuated briefly. Then 0.2 bar propanamine was admitted, allowed to adsorb for 0.3 ks, and finally evacuated for 0.6 ks. A carrier gas flow (100 cm^3/min) was then established and the sample purged for 0.6 ks prior to TA.

Propanamines were reacted at constant temperature in a gradientless recirculating batch reactor system described elsewhere (30). Catalyst (100 mg) was placed in a quartz reactor between two quartz wool plugs. The circulation loop was equipped with a magnetically operated piston pump and check valve arrangement, and the entire system could be evacuated. The system pressure was monitored with a diaphragm-type pressure gauge. In a typical experiment, the catalyst was first dried under vacuum under the same thermal conditions as employed in the microbalance. Then He was admitted to the reactor section at just above atmospheric pressure and the reactor was isolated. The circulation loop was filled with 0.015 bar propanamine and 1.1 bar He and a GC analysis was performed prior to contact with the catalyst. The reaction was started by diverting the circulating mixture through the reactor, equilibrated at the reaction temperature. Samples were withdrawn periodically through a traced line to an evacuated loop on a gas sampling valve. The GC was an HP5890 II equipped with a 50-m PONA capillary column and FID detector. Identification of components was by syringe injection of pure standard samples and by offline sampling into a GC–MS system. Offline samples from the TA experiments were also injected by gas syringe into the GC–MS system.

RESULTS

H–MFI Sample

Microbalance curves depicted in Fig. 1 represent the isothermal transient 1-PA adsorption process when the reagent gas flow is switched through the 1-PA bubbler. A separate experiment using DPA is also depicted and will be discussed below. In each case, the switch to deliver 1-PA to the zeolite sample occurred after 0.06 ks. Rapid weight gain occurred immediately, with saturation reached after about 0.09 ks for 1-PA. The saturation value at 323 K corresponds to somewhat less than three 1-PA molecules per Al atom of the zeolite, which suggests that almost the entire zeolite pore volume, estimated to be 0.178 cm^3/g (17), was filled with 1 -PA. The replacement of half of the He reagent gas with H_2 did not change the saturation value but perhaps accelerated the adsorption process slightly. When the bubbler was then bypassed at 0.36 ks, there was a slow weight decline attributed to the

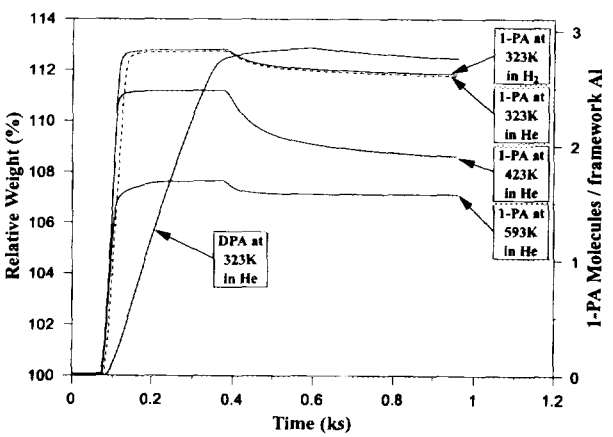

FIG. 1. Transient adsorption of 1-PA and DPA on H–MFI.

isothermal desorption of weakly bound 1-PA. Increasing the adsorption temperature to 423 K led to about a 10% decrease in the total amount adsorbed and noticeably accelerated the rate of the isothermal desorption beginning at 0.360 ks without noticeably affecting the initial rate of adsorption. A further increase in the adsorption temperature to 593 K, however, did not result in a decrease in the amount of adsorption to one 1-PA molecule per framework aluminum; the observed behavior was unexpected since 593 K is the "plateau" region reported by Gorte and co-workers (17) where the propylammonium cation is stable. Instead, the maximum weight of the sample at 593 K corresponded to 1.7 1-PA molecules per Al atom, and declined to 1.6 1-PA molecules per Al during the purge with pure He.

The TA and DTA data presented in Fig. 2 clearly indicate that neither a change in the carrier gas nor an increase in the adsorption temperature from 323 to 423 K had an effect on the subsequent desorption and reaction of 1-PA, since virtually indistinguishable TA and DTA curves were obtained. The expected plateau related to the formation of the 1 : 1 stoichiometric complex (17) was still present in all cases and the major desorption feature at 672 K was observed in accordance with the literature. However, radical changes in the TA features occurred when 1-PA was adsorbed at 593 K. Figure 2 shows that the major desorption feature shifted to a higher temperature compared to the experiments following 323 and 423 K adsorption. In addition, the sample weight in the "plateau" region is equivalent to 1.7 1-PA molecules/framework Al instead of the one molecule/framework Al which was observed when adsorption occurred at 323 or 423 K. Furthermore, two unresolved features are visible at 703 and 743 K in the DTA curve instead of a single major feature at 672 K and a minor feature at 743 K.

Our assessment of these observations is that, at the higher adsorption temperature, the 1-PA in the gas phase can react with propylammonium ions already formed on the zeolite. The dipropylammonium cation is a probable product of such an interaction and is consistant with the weight gain which is equivalent to 1.7 1-PA molecules, and this hypothesis was tested in separate experiments with a DPA adsorbate. Returning to Fig. 1, where the transient DPA response curve is compared to the 1-PA response curves, virtually the same saturation coverage is noted for both 1-PA (adsorbed at 323 K) and DPA, suggesting that the entire pore volume of the H–MFI sample was filled in both cases. The adsorption of DPA was slower due to the larger size and consequently lower diffusivity of the DPA molecule in the narrow zeolite pores. Subsequent TA of DPA (Fig. 2) revealed that desorption of weakly bound DPA proceeds much as 1-PA desorption up to about 425 K, then the DPA coverage remains almost constant to about 675 K, where the major features begin. The TA curves above 675 K are very similar for both 1-PA adsorbed at 593 K and DPA adsorbed at 323 K, and this observation provides further evidence that the adsorption of 1-PA at 593 K results in the formation of dipropylammonium cations. Note also that in both cases the sample weight returns to the original weight above 800 K, which means that all products were desorbed.

The extensive work of Gorte and co-workers (14–17) focused on the interaction of propanamines with the pro-

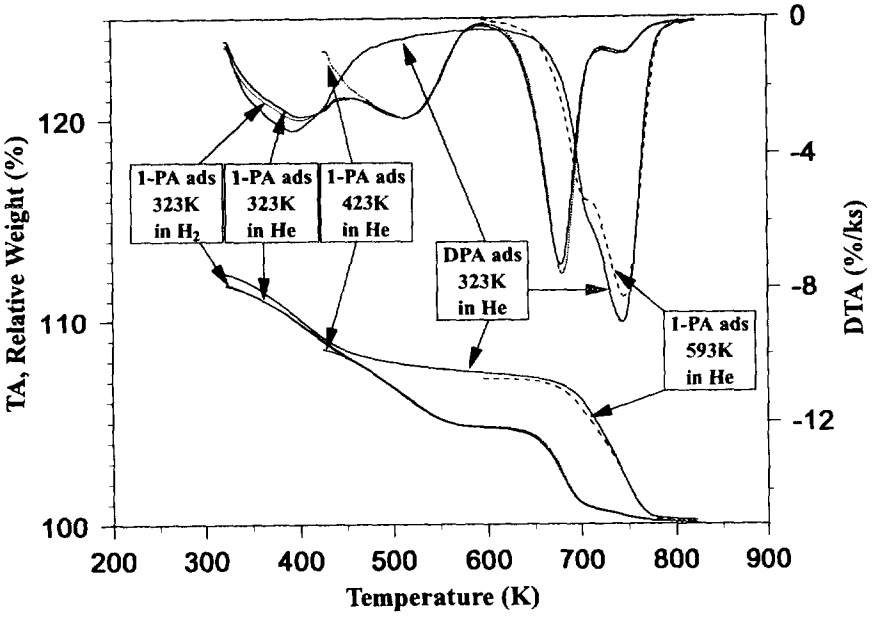

FIG. 2. Thermal analysis (upper: DTA; lower: TA) of adsorbed 1-PA and DPA on H–MFI.

ton acid sites of the zeolite at relatively low coverage. Along with the 1 : 1 stoichiometric complex of propanamine with zeolitic protons, the authors also reported a low temperature desorption state that they suggested was not associated with acid sites (14), although the interaction of propanamine with the internal silanols of the zeolite was not excluded (17). In our previous study (28), we observed two distinct low temperature features for propanamine desorbing from H–MFI, and have suggested that they are indirectly related to the acid sites through formation of "solvation shells" surrounding the propylammonium cations. In this investigation, we confirm the close relationship between the adsorption states of propanamine at low and high temperatures. In Fig. 2, neither the shape nor the intensity of the 509 K low temperature feature on the DTA curves for 1-PA changes when the 1-PA desorption temperature is changed from 323 to 423 K. The weight change corresponding to this feature is still roughly one 1-PA molecule per framework Al. Moreover, this feature is missing completely when DPA is adsorbed at 323 K. If simple physical adsorption or interactions with internal silanols cause the adsorption state corresponding to the 509 K feature, then the feature would also be observed when DPA was adsorbed, because of DPA's higher boiling point and basicity. We believe the absence of the feature at 509 K in the desorption of DPA is due to steric constraints which restrict a second DPA molecule from interacting with the acidic hydrogen atoms. This postulate is consistent with the zeolitic pore capacity at full saturation of DPA (at 323 K), which is about 1.5 DPA molecules per framework Al.

The high temperature features in Fig. 2 are due to decomposition of the complexes formed in the "plateau" (600–625 K) region of the TA curves, while the low temperature (<600 K) features are due to desorption of the unreacted adsorbate. This was determined by MS analyses. When 1-PA is adsorbed at low temperatures (323 or 423 K) the 672 K feature accounts for about 85% of the high temperature features, while the remainder desorbs around 743 K. For 1-PA adsorbed at 593 K, the 672 K feature disappears and the 732 K feature dominates, although a shoulder at 703 K is present.

These observations about the adsorption–desorption features of propanamines can be rationalized by a simple reaction scheme which is consistent with well-known amine chemistry and the properties of H–MFI as a solid Brønsted acid:

$$C_3H_7NH_2 + H^+Z^- \rightarrow C_3H_7NH_3^+Z^- \quad [2]$$

$$C_3H_7NH_2 + C_3H_7NH_3^+Z^- \rightarrow C_3H_7NH_2 \cdots C_3H_7NH_3^+Z^- \quad [3]$$

$$C_3H_7NH_2 \cdots C_3H_7NH_3^+Z^- \rightarrow (C_3H_7)_2NH_2^+Z^- + NH_3 \quad [4]$$

$$(C_3H_7)_2NH + H^+Z^- \rightarrow (C_3H_7)_2NH_2^+Z^- \quad [5]$$

$$C_3H_7NH_3^+Z^- \rightarrow C_3H_6 + NH_3 + H^+Z^- \quad [6]$$

$$(C_3H_7)_2NH_2^+Z^- \rightarrow 2C_3H_6 + NH_3 + H^+Z^- \quad [7]$$

$$(C_3H_7)_2NH_2^+Z^- \rightarrow C_3H_6 + C_3H_7NH_2 + H^+Z^-. \quad [8]$$

The interaction of 1-PA with the zeolitic protons leads to formation of the propylammonium ion (reaction [2]) as has been proven in numerous previous investigations (14–17). The propylammonium cation can also interact with 1-PA molecules (reaction [3]). The desorption of the first shell of 1-PA molecules around propylammonium cations is responsible for the feature at 509 K; the molecules can be desorbed without decomposition. If 1-PA is present in the gas phase while the temperature is raised, reaction [3] is forced to the right, leading to the formation of the dipropylammonium cation with the evolution of NH_3 (reaction [4]) at higher temperatures. The DPA cation can also be formed by direct adsorption of DPA (reaction [5]), even at low adsorption temperatures. Some of the possible

TABLE 1

Hydrocarbon Product Composition during TA of 1-PA and DPA

	1-PA adsorbed at 593 K			DPA adsorbed at 323 K	
Sampling temperature (K)	593	703	748	593	775
Total of GC peak areas	0	3733	6676	0	5943
Product distribution (Area %):					
Ethene	—	2.20	0.48	—	2.15
Ethane	—	0.75	0.00	—	0.00
Propene	—	92.34	96.27	—	95.81
Propane	—	0.67	0.49	—	0.66
1-Butene + isobutene	—	1.79	1.02	—	0.71
trans-2-Butene	—	1.23	1.06	—	0.42
cis-2-Butene	—	1.02	0.67	—	0.25

pathways for decomposition of the adsorbed propylammonium and dipropylammonium ions upon temperature programming are represented by reactions [6]–[8].

The proposed reaction scheme is in accordance with the properties of alkylamines as bases. It is known that the basicity and thus the strength of the interaction with Brønsted sites increases in the sequence NH_3 < primary < secondary. Therefore the dipropylammonium ion should be the most stable surface species under our experimental conditions and should decompose at a higher temperature than the propylammonium ion. DTA curves, however, show that in the case of 1-PA desorption a small feature at 743 K characteristic of the dipropylammonium cation is present. This peak might result from the desorption of dipropylammonium ions which have formed through the reaction of readsorbing 1-PA with 1-propylammonium cations. Interactions of 1-PA with Lewis acid sites of the zeolite might also be responsible for this feature, as we will subsequently show.

Further analyses of the decomposition products of 1-PA and DPA have been performed for confirmation purposes. These included flow reactor experiments with mass spectral analysis of the reactor effluent, analysis of samples taken directly from the microbalance and the flow reactor, and, finally, the investigation of the conversion of 1-PA catalyzed by H–MFI at 593 K in a batch recirculating reactor.

Table 1 details results of chromatographic sampling of the microbalance effluent during TA of adsorbed 1-PA and DPA. Sampling temperatures were chosen to correspond to important events which occur during TA: 593 K to the "plateau" region where no desorbing species are expected; 703 K to the shoulder on the main desorption peak; 748 K (approximately) to the maximum in the main peak; 775 K to the region just past the maximum. In all cases, propene was observed at over 90% abundance and only traces of other olefins and a few paraffins were observed. NH_3 is also expected but the GC detector does not respond to this molecule.

The bimolecular reaction of gas phase 1-PA with the adsorbed propylammonium cation to make the DPA cation was investigated in more detail using a batch recirculation reactor. We introduced 1-PA in an amount equivalent to about six 1-PA molecules per framework Al in the catalyst sample. The product distribution for the conversion of 1-PA at 593 K is shown as a function of time in Fig. 3.

The product data confirm the formation of DPA as the major reaction in the conversion of 1-PA over H–MFI. The DPA yield goes through a maximum due to formation of hydrocarbons and heavier products at long contact times. Only small amounts of nitriles and tripropylamine appear. The C_6-imine (*N*-propylidenpropylamine) yield parallels that of DPA but is only one-tenth the DPA yield at identical reaction times. GC–MS has been used in an

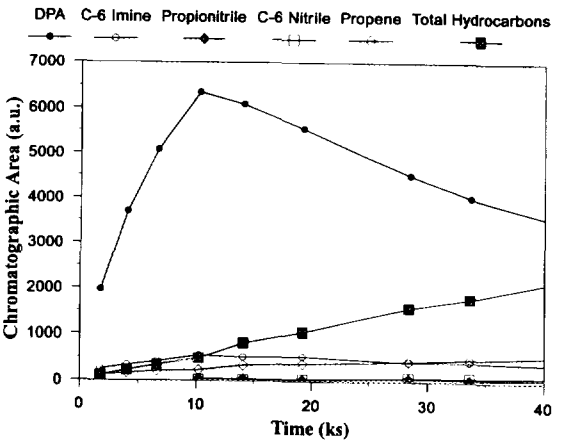

FIG. 3. 1-PA conversion in batch recirculation reactor catalyzed by H–MFI at 593 K. (●) DPA; (○) C_6-imine; (◆) propionitrile; (□) C_6-nitrile; (◇) propene; (■) total hydrocarbons.

effort to further identify this product; a definitive identification has thus far eluded our efforts, but the following characteristics are important:

1. The most intense ion is located at m/e = 70 which is 2 m/e units lower than the most intense ion in DPA.
2. Ions at m/e = 99, 71, 56, and 28 are also shifted 2 units lower than the corresponding DPA ions at m/e = 101, 73, 58, and 30.

An imine would be a relatively stable product of DPA dehydrogenation. The formation of such alkylidenalkylamines has been previously reported during the catalytic conversion of alkylamines on alumina (31, 32); thermal pretreatment of the alumina, leading to an increase in Lewis acidity, resulted in an increase in selectivity for the formation of the imine product (31). The occurrence of dehydrogenation reactions of 1-PA on H–MFI zeolite is further established by the presence of small amounts of propionitrile and another C_6-nitrile among the reaction products at higher contact times. At present, we do not fully understand the mechanism of this dehydrogenation reaction over the strongly acidic H–MFI catalyst, although subsequently we show that the replacement of zeolite protons with other cations accelerated 1-PA dehydrogenation. Therefore, in addition to reactions [2]–[8], the following dehydrogenation routes should be included as important reactions of 1-PA catalyzed by H–MFI.

$$2C_3H_7NH_2 \rightarrow CH_3CH_2CH = N - CH_2CH_2CH_3 + NH_3 + H_2 \quad [9]$$

$$(C_3H_7)_2NH \rightarrow CH_3CH_2CH = N - CH_2CH_2CH_3 + H_2 \quad [10]$$

$$C_3H_7NH_2 \rightarrow CH_3CH_2CN + H_2 \quad [11]$$

$$2C_3H_7NH_2 \rightarrow C_2H_5CN + C_3H_6 + 2H_2 + NH_3 \quad [12]$$

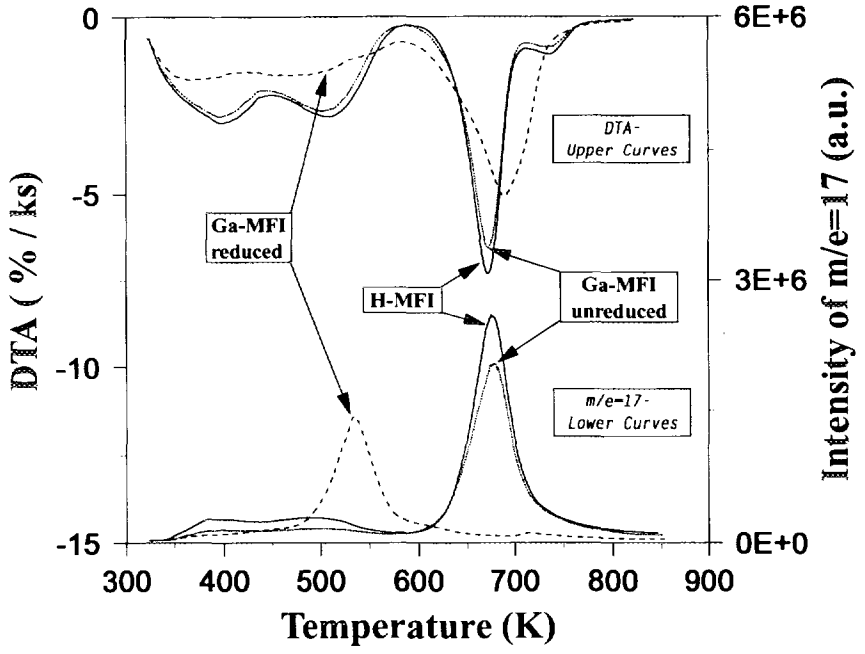

FIG. 4. Thermal analysis (upper: DTA; lower: m/e = 17) of 1-PA on H–MFI and unreduced and reduced Ga–MFI.

$$2C_3H_7NH_2 \rightarrow C_5H_{11}CN + NH_3 + 2H_2. \quad [13]$$

The results shown in Fig. 3 also indicate that hydrocarbon formation was slow compared to DPA formation. Propene appeared as the first hydrocarbon product, and as the reaction proceeded, hexenes were formed probably through dimerization routes. C_6 hydrocarbons were the dominant products at a contact time of 82.5 ks. Two pentene isomers (*trans*-2-pentene and *cis*-2-pentene) were also present in appreciable amounts, whereas no butenes and only traces of ethene could be detected even at very high contact times.

Many of these interactions of 1-PA with H–MFI are either well known or unsurprising given the strong Brønsted acidity of H–MFI. From this point, our interest was in determining whether 1-PA is exclusively a probe of Brønsted acidity, or if similar reactions took place when protons were replaced with other cations. This has led to a study of Ga–, In–, and Cu–MFI all prepared in a manner such that proton replacement was expected. Results of TA and catalytic reactor experiments follow.

Ga–MFI Sample

The Ga-containing catalyst used in this investigation was produced by intense mechanical mixing of H–MFI with Ga_2O_3. Previously, we studied a Ga-impregnated MFI catalyst (Ga–MFI(imp)) and found that the presence of gallium affects the decomposition chemistry of both 1-PA and 2-propanamine (2-PA) (28, 33). Gallium impregnation led to some ion exchange during the calcination procedure, so we have chosen the mechanically mixed catalyst as a model system for characterization studies that allows two well-defined states of the catalyst. Before reduction with hydrogen, the catalyst contains only the proton (Brønsted) acid sites of the H–MFI, since the gallium oxide phase was shown to be virtually inert with respect to 1-PA. After high temperature reduction with H_2, however, all the protons of the H–MFI sample were replaced by reduced Ga^+ ions (34–35); therefore the reduced catalyst contains only reduced Ga ions, which may be considered Lewis acid sites. The preliminary results on the mechanically mixed Ga–MFI catalyst indicated that the reduction of the catalyst played a key role in changing its interaction with propanamines (33). In the present study, we further examine and explain the new mode of 1-PA decomposition due to the presence of Ga cations in the zeolite.

Figure 4 presents a comparison of the microbalance DTA data with TA data obtained using the flow reactor, for the TA of 1-PA. There is virtually no difference in the behavior of the H–MFI catalyst and the unreduced Ga–MFI sample, except that slightly lower intensities are observed for the Ga-containing material because unreduced gallium oxide behaves essentially as an inert diluent. In contrast, there are dramatic changes in both the microbalance DTA and the m/e = 17 (ammonia) TA curves after hydrogen reduction. The low temperature DTA features at 403 K and 509 K diminish sharply, and the major DTA feature shifts from 678 to 689 K and changes in shape. More importantly, a new feature at 534 K (134 K lower than H–MFI) appears in the MS–TA results, with

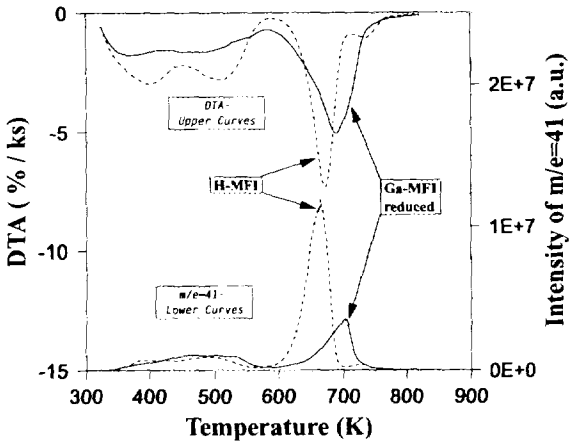

FIG. 5. Thermal analysis (upper: DTA; lower: m/e = 41) of 1-PA on H–MFI and reduced Ga–MFI.

complete NH_3 desorption from the reduced catalyst between 500 and 600 K. The integrated MS intensity of the ammonia peak for the reduced sample is markedly lower than that evolved by unreduced Ga–MFI. Figure 5 is similar to Fig. 4 except that it highlights the MS–TA results for m/e = 41 (characteristic of propene), showing clearly that reduction also strongly affects propene evolution. The main m/e = 41 peak is shifted to a higher temperature and is much lower in intensity for the reduced Ga–MFI sample.

The weight change calculated as 1-PA molecules per framework Al during TA of 1-PA is depicted in Fig. 6. The formation of the 1 : 1 stoichiometric complex is easily seen for the H–MFI sample, but different features are observed for the reduced Ga–MFI sample. The entire Ga–MFI curve lies above the curve for H–MFI except for a slight capacity difference in the pore filling region below 400 K. Even after complete desorption of ammonia from the reduced catalyst (by 600 K, see Fig. 4), the equivalent of 1.32 molecules of 1-PA are still held on the reduced catalyst. This feature resembles that observed for H–MFI when 1-PA was adsorbed at 593 K or DPA was adsorbed at 323 K, and consequently can be explained as the formation of different kind of complex between 1-PA and gallium cations in the zeolite. Another characteristic feature of desorption from a reduced Ga–MFI sample is the appearance of a residue, as detected by the stable weight offset at the conclusion of the TA experiment. The residue is equivalent to 0.25 1-PA molecules for each Al atom of the sample. Further microbalance experiments helped establish that this weight offset cannot be removed by prolonged heating in He at 848 K but a short treatment in the H_2/He mixture at 848 K was sufficient to return the sample weight to its initial value. This suggests that the formation of the residue (and likely the whole process of 1-PA thermal analysis) is strongly influenced by dehydrogenation reactions.

To further investigate the changes in amine chemistry associated with reduced Ga, we performed microbalance TA experiments with a mechanically mixed catalyst which contained only half as much gallium as the standard Ga–MFI (1 : 1 Ga/Al). The results of TA experiments with the half-loaded sample were compared with a standard sample which had been reduced to only half its full reduction potential. This was achieved by simply cutting off the H_2 supply during the reduction process at a point where half the total expected weight loss had been reached. Figure 7 compares H–MFI, half-loaded Ga–MFI (0.5 Ga–MFI), and the half-reduced Ga–MFI. Half reduction of Ga–MFI does not lead to complete removal of the primary desorption feature of 678 K which is characteristic of desorption from Brønsted sites. Instead, two high temperature features of similar intensity at 681 and 712 K are present, strongly suggesting the separate interaction of 1-PA with both the protons and the Ga ions of the zeolite. The DTA curve for the half-loaded Ga–MFI is quite similar to the half-reduced material. The raw TA curve for the half-reduced material lies slightly below the half-loaded material, but this is due to the unreacted Ga_2O_3 of the former, which continues to act as virtually an inert diluent. These results support our hypothesis that Ga ions and zeolitic protons interact separately with 1-PA.

Figures 8–10 compare 1-PA thermal analysis in He versus H_2/He reagent gas. Apparently, hydrogen suppresses residue formation during TA of 1-PA, as the sample weight returns to its initial value at the completion of the 1-PA TA experiment when H_2 is present (Fig. 8). Major changes also occur in the composition of the desorbing gas, as represented by the characteristic masses shown in Figs. 9 and 10. The peak for m/e = 54 (characteristic of nitriles) is sharper and diminishes by 31% when H_2 is present. Much more total ammonia (m/e = 17) is desorbed in a hydrogen atmosphere (Fig. 9), particularly in the ammonia peak at 708 K and the shoulder at about 580 K. These

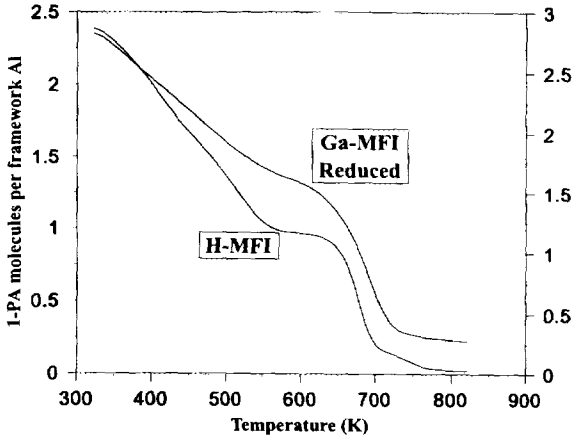

FIG. 6. Thermal analysis of 1-PA on reduced Ga–MFI and H–MFI.

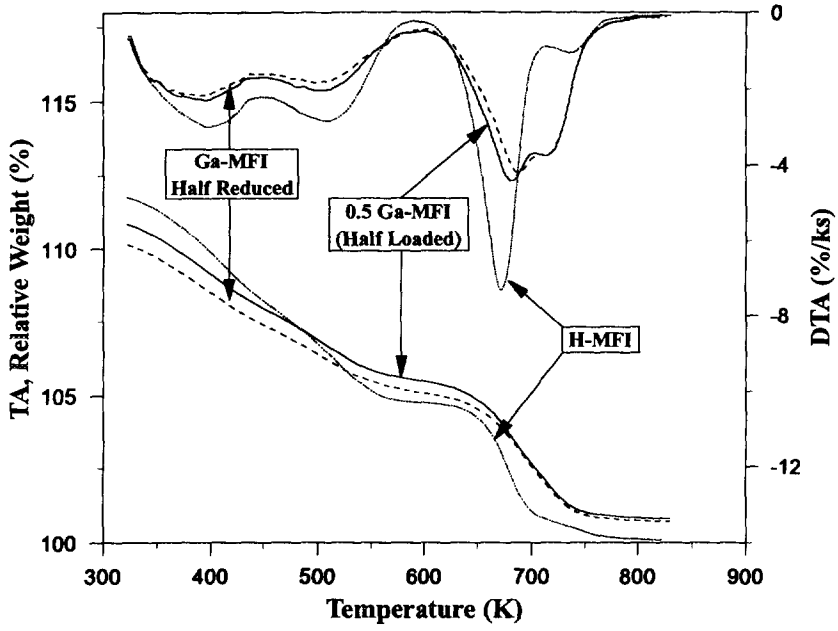

FIG. 7. Thermal analysis (upper: DTA; lower: TA) of 1-PA on H–MFI, reduced 0.5 Ga–MFI, and half-reduced Ga–MFI.

peaks are completely absent for the reduced Ga–MFI when the He reagent gas was used. Significant changes also occur in the $m/e = 41$ peak characteristic of propene (Fig. 10), whose intensity is about three times greater, using the H_2/He reagent gas, for reduced Ga–MFI. Hydrogen affected 1-PA decomposition only in the case of the reduced Ga–MFI sample, as no effects were observed with the pure H–MFI sample. The influence of hydrogen cannot be investigated using unreduced Ga–MFI because the presence of H_2 would lead to reduction of the Ga_2O_3 component.

The effects of hydrogen most likely have simple kinetic explanations. Imine formation (reactions [9] and [10]) and nitrile formation (reactions [11]–[13]) involve the production of H_2 and, if these reactions are reversible, would be retarded by the presence of H_2 in the reagent gas. This is what is observed. The Hofmann eliminations do not produce H_2 and so the selectivity for these reactions is enhanced by the presence of H_2. This situation is similar to paraffin dehydrocyclization, where the rate-limiting step is the recombinative desorption of H_2 (36), and the reactions are therefore inhibited by gas-phase H_2 (37, 38).

The curves for $m/e = 17$ (Fig. 9) and the results for residue formation (Fig. 8) support this interpretation. Ammonia production would be expected to decrease as nitrile and imine production increases; this is what was observed. Imines and nitriles can easily undergo secondary reactions resulting in the formation of heavier products which eventually produce a residue, which is the case when He was the reagent gas. The analysis of the flow reactor effluent by GC further confirms the role of dehydrogenation reactions during 1-PA thermal analysis. Selected GC data summarized in Table 2 show the products of 1-PA decomposition on the unreduced Ga–MFI sample as consisting mainly of propene and small quantities of other light hydrocarbons produced by side reactions. When the same experiment is conducted on reduced Ga–MFI in He, a large amount of propionitrile is produced. But the use of H_2 as a carrier gas during the TA experiment increases the propene/nitrile ratio markedly.

The catalytic data taken using the batch recirculation reactor with Ga–MFI(imp) (Fig. 11 and Table 3) provide further evidence of a new mode of interaction for 1-PA with reduced Ga–MFI. These 1-PA reactor experiments

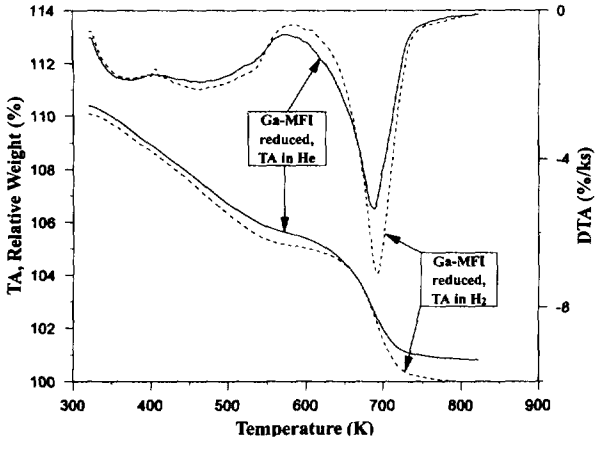

FIG. 8. Thermal analysis (upper: DTA; lower: TA) of 1-PA on reduced Ga–MFI in He and H_2/He.

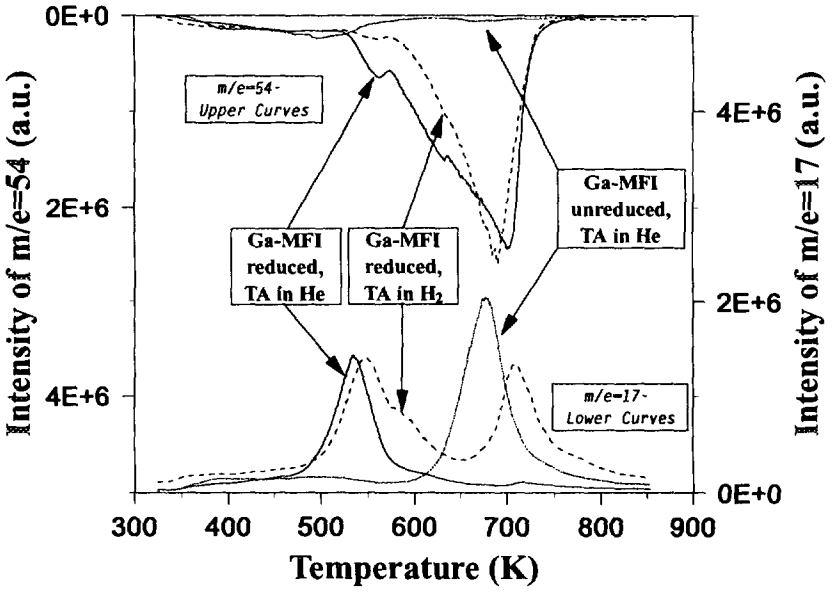

FIG. 9. Comparison of ions characteristics of nitriles (m/e = 54) and NH_3 (m/e = 17) during thermal analysis of 1-PA in He and H_2/He on Ga–MFI.

were performed under the same conditions as in the case of the H–MFI sample (Fig. 3). Figure 11 shows that, analogous to the H–MFI sample, the formation of DPA is the primary process occurring at low contact times. Ga–MFI(imp) differs from H–MFI in that C_6-imine (N-propylidenpropylamine) is produced in large quantities and in that it appears to be an initial product of 1-PA conversion. As the reaction proceeds, propionitrile eventually becomes the major product and the formation of a C_6-nitrile increases steadily along with the production of hydrocarbons. The detailed product distribution (Table 3) shows that even at the highest contact times there are only traces of saturated hydrocarbons and no C_4 hydrocarbons, and branched alkenes are limited to traces of branched C_6 compounds. In these ways reduced Ga–MFI was similar to H–MFI. The most pronounced difference

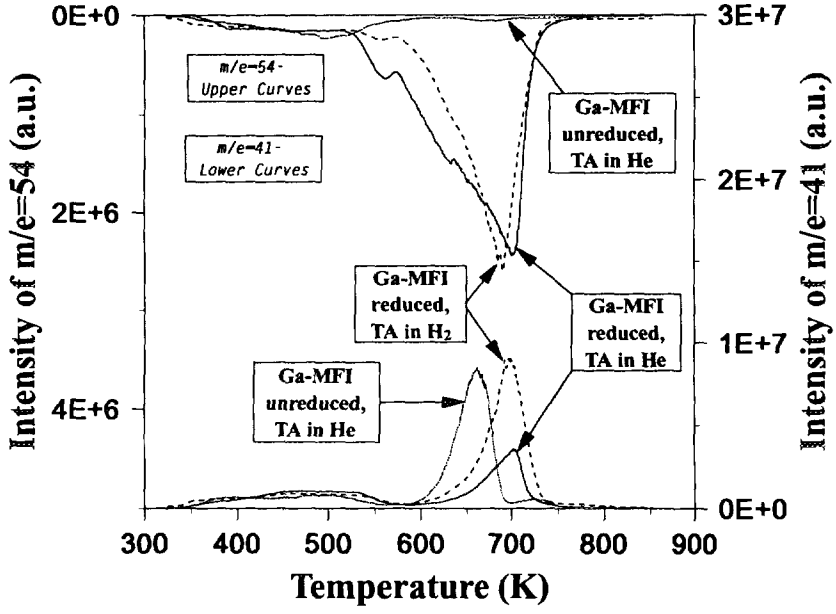

FIG. 10. Comparison of ions characteristic of nitriles (m/e = 54) and propene (m/e = 41) during thermal analysis of 1-PA in He and H_2/He on Ga–MFI.

TABLE 2

Product Composition during TA of 1-PA over Ga–MFI

	Unreduced Ga–MFI, TA in He	Reduced Ga–MFI, TA in He		Reduced Ga–MFI, TA in H_2		
Sample Temperature (K)	673	573	683	573	668	783
Methane						6.11
Ethene	0.82	1.51	1.92		0.77	5.89
Ethane			0.46			
Propene	91.38	12.37	38.51	33.50	57.37	49.80
Propane			0.60	4.37	1.08	3.25
1-Butene	0.49		1.32		0.33	1.12
trans-2-Butene	0.21		0.68		0.18	2.58
cis-2-Butene	0.17		0.50		0.14	1.40
3-Methyl-1-butene			0.25			
1-Pentene			0.74		0.23	
2-Methyl-1-butene			0.77		0.55	
trans-2-Pentene			1.65		0.46	
1-Pentyne			0.39			
cis-2-Pentene			0.88		0.27	
2-Methyl-2-butene			1.72		1.04	
1-Hexene			0.47		0.40	
Other hexenes	0.45		5.22		2.06	
Benzene	0.47		1.20		1.16	3.03
Toluene			0.40		0.41	3.08
1-PA	6.00					
Acetonitrile						9.20
Propionitrile		86.12	42.33	62.14	33.97	14.53

TABLE 3

Products of the Catalytic Reaction of 1-PA over Ga–MFI(imp) at 593 K

Time (ks)	0	1.80	4.02	6.60	10.2	13.2	16.6	23.6	52.8	80.1	150
Total peak area	32963	14000	14147	14804	13465	13262	13621	13277	12669	11563	11500
Production distribution											
Hydrocarbons:											
Ethene								0	0	24	38
Propene		199	245	306	410	416	429	528	682	724	1043
Propane						36			81	72	112
Pentene-1							18	0	33	27	77
trans-Pentene-2			43	55	76	89	117	154	252	299	530
cis-Pentene-2			31	44	51	56	57	84	120	160	266
Hexene-1			43	55	86	97	101	130	216	264	428
Other hexenes			0	20	82	86	109	140	275	336	884
Total hydrocarbons		199	352	480	705	780	831	1036	1659	1906	3378
N-containing compounds:											
1-PA		4340	3291	3578	2772	2112	2050	1700	1800	1400	300
DPA		6945	7044	6594	5622	5111	4801	4203	2396	1286	100
Tripropylamine		43	134	221	266	330	361	384	375	211	98
C_6-Imine		1519	1518	1472	1374	1366	1331	1340	888	573	55
Propionitrile		555	1162	1642	2079	2580	2945	3395	3856	4339	5271
C_6-Nitrile		45	115	203	294	383	453	601	933	1217	1961
Heavier nonidentified:											
26.595[a]		43	54	64	64	79	111	89	96	47	77
27.946[a]		108	234	292	253	352	418	349	297	226	144
28.785[a]		24	47	15	0	0	0	0	0	0	0

[a] Retention time (min).

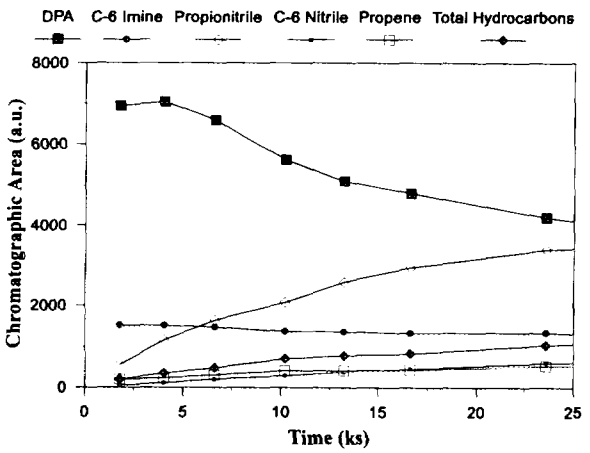

FIG. 11. 1-PA conversion catalyzed by reduced Ga–MFI at 593 K. (■) DPA; (●) C_6-imine; (◇) propionitrile; (▪) C_6-nitrile; (□) propene; (◆) total hydrocarbons.

between H–MFI and reduced Ga–MFI lies in the promotion of specific dehydrogenation reactions by the latter (reactions [11]–[13]).

The appearance of the C_6-nitrile deserves special consideration. First, the exact identity of this compound is somewhat in question. Identification efforts by GC–MS showed that, according to its fragmentation pattern, the compound could possibly be 4-methylpentanenitrile but the fit parameters were not good. Additional verification efforts with pure hexanenitrile and 4-methylpentanenitrile as GC standards showed that neither compound matched the retention time of the observed C_6-nitrile. However, a good correlation was obtained between the boiling points and the measured retention times of 4-methylpentanenitrile and hexanenitrile on the PONA capillary column used for GC analysis. According to this correlation, the "unknown" C_6-nitrile would have the boiling point of 2-methylpentanenitrile. Unfortunately, a pure sample of this isomer is not readily available and we have been unable to find a mass spectrum of this particular isomer in the literature. Thus, we tentatively identify the C_6-nitrile as 2-methylpentanenitrile.

We assume based on the TA and catalytic data that two 1-PA molecules can be coordinated and strongly held to the Ga cations in the zeolite. The close proximity of both 1-PA molecules and the intrinsic activity of the Ga cations leads to a transalkylation reaction. The DPA product remains adsorbed on the Ga cation, although the product ammonia is desorbed at a temperature as low as 550 K. Upon further temperature increase, dehydrogenation reactions begin, and the extent to which these reactions occur depends not only on the temperature but also on the presence of 1-PA and hydrogen in the gas phase. The formation of adsorbed C_6-imine (*N*-propylidenepropylamine) is probably the first dehydrogenation reaction (see Fig. 11). The adsorbed species can then decompose under the conditions of thermal analysis yielding propionitrile and propene. On the other hand, we cannot exclude the direct dehydrogenation of adsorbed 1-PA to a very reactive imine that easily reacts further to produce heavier N-containing compounds which remain on the catalyst and constitute residue precursors. Under the conditions of the catalytic experiment, DPA and the C_6-imine are desorbed as primary products, and, as the reaction proceeds, propionitrile, propene, and other hydrocarbons (mainly C_5 and C_6 olefins) are produced.

In–MFI

Because the existence of reduced Ga cations in the zeolite appears to be responsible for the altered product distribution in the reactions of 1-PA, it is important to investigate the catalytic behavior of other reducible post-transition metal cations for reactions of amines. Therefore, we have also investigated MFI zeolites containing In and Cu cations prepared in a manner which allows comparison to the Ga–MFI system.

In a previous report, the reduction of In_2O_3/H–MFI mechanical mixtures with H_2 resulted in a process of solid state ion exchange analogous to Ga_2O_3/H–MFI; In ions were introduced into cationic positions of the zeolite. This process has been found to occur more readily with In than with Ga and therefore 623 K is a sufficient reduction temperature (39). Thermal analysis of 1-PA over reduced In–MFI is shown in Fig. 12. The ion at m/e = 59 is the parent ion of 1-PA. Note that the In–MFI sample desorbs much more unreacted 1-PA at $T < 600$ K than Ga–MFI; therefore, not only are the NH_3 and propene peaks smaller compared to the peaks for unreacted 1-PA, but the fragmentation background contributions from 1-PA to masses 17 and 41 are also much stronger and so the spectra appear

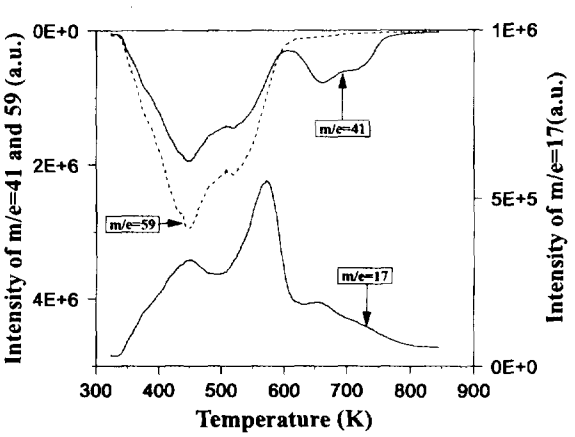

FIG. 12. Ions characteristic of NH_3 (m/e = 17), propene (m/e = 41), and 1-PA (m/e = 59) during thermal analysis of 1-PA on reduced In–MFI.

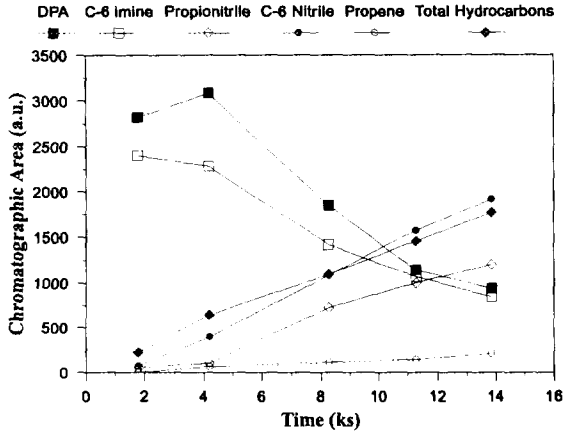

FIG. 13. 1-PA conversion catalyzed by reduced In–MFI at 593 K. (■) DPA; (□) C_6-imine; (◇) propionitrile; (●) C_6-nitrile; (○) propene; (◆) total hydrocarbons.

different from the Ga–MFI case. One can see, however, that a strong ammonia desorption peak is present in the temperature range 500–600 K, and the high temperature (>600 K) desorption peaks of m/e = 41 are shifted to a higher temperature than is the case for H–MFI; this result is similar to that obtained using the reduced Ga–MFI catalyst. Initial (323 K) coverages of 1-PA on In–MFI and Ga–MFI are also similar.

The product distribution as a function of time for the batch conversion of 1-PA catalyzed by reduced In–MFI is shown in Fig. 13. The initial conversion of 1-PA is directed to DPA and a C_6-imine as the primary products. Much less C_6-nitrile and propionitrile are produced compared to Ga–MFI and the formation of hydrocarbons is also suppressed. It appears that the unique feature of the reduced In-containing catalyst is its ability to accelerate the formation of the C_6-imine compared to both the H–MFI and the reduced Ga–MFI catalysts.

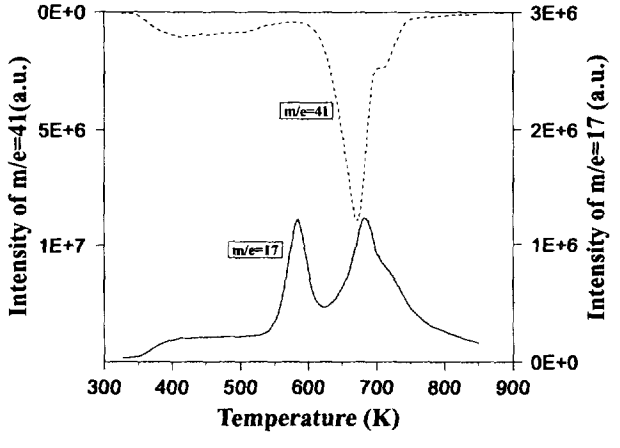

FIG. 14. Ions characteristic of NH_3 (m/e = 17) and propene (m/e = 41) during thermal analysis of 1-PA on Cu–MFI.

Cu–MFI

Recent results (e.g., (40)) suggest that Cu cations can be introduced into cationic positions in MFI when mechanical mixtures of CuO and H–MFI zeolite are heated in vacuum or flowing inert gas. We applied this approach to produce a Cu–MFI catalyst that was subjected to both 1-PA thermal analysis in the flow reactor and 1-PA catalytic conversion in the batch recirculating reactor. Separate experiments with a pure CuO sample verified that the copper oxide does not adsorb 1-PA to any appreciable extent at 323 K. It is important to note that no hydrogen reduction was applied in the production of the copper-containing catalyst, because treatment with hydrogen at elevated temperatures would lead rapidly to the reduction of CuO to Cu prior to its transfer into the zeolite. Under heat treatment in vacuum, we expect the spontaneous reduction of CuO to Cu_2O followed by transfer of Cu^+ ions into the zeolite. The spontaneous reduction requires temperatures of 900 K or more in the absence of O_2, which is higher than the temperatures tested by Karge *et al.* (40), so we have used 973 K as a pretreatment temperature in pure He.

The m/e = 17 and m/e = 41 mass spectral peaks during 1-PA TA are shown in Fig. 14. Ammonia evolves as two distinct peaks at low (550–600 K) and high (650–750 K) temperature while only one peak for m/e = 41 is observed. As we pointed out in the cases of Ga–MFI and In–MFI, the appearance of an ammonia desorption peak at low temperatures indicates that bimolecular reactions are operative during the initial transformation of adsorbed 1-PA. These data might appear in direct contrast to the data of Parrillo *et al.* on Cu-containing MFI (18), but they studied 2-propanamine desorption, which sterically hinders the bimolecular reactions. Product distribution data from the batch recirculation reactor, presented in Figure 15 and Table 4, show that 1-PA conversion on the Cu–MFI catalyst leads largely to nitriles and hexenes during the initial stages of the reaction. In contrast to all other catalysts under investigation, the C_6-nitrile is the primary reaction product with a concentration of about twice that of both propionitrile and hexenes. Only small amounts of DPA and C_6-imine are present among the products even at contact times less than 1.8 ks. No methane could be detected. The hydrocarbon content continues to increase at high contact times and reaches 83% of the products at 254 ks. There are characteristic changes in the hydrocarbon composition as the reaction proceeds. No saturated hydrocarbons are present except for traces of ethane and propane at high contact times. Branched alkenes (e.g., 2-methylpentene-2 and 2-methylpentene-1) appear among the products at long contact times. In addition, the changes in the total reactor content represented by the total peak area (Table 4) suggest that, initially, a catalyst

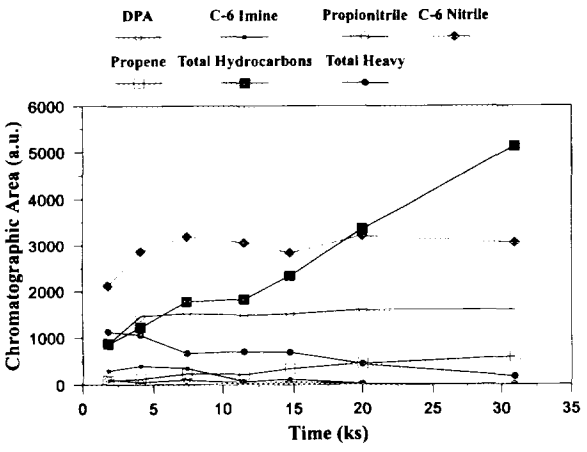

FIG. 15. 1-PA conversion catalyzed by Cu–MFI at 593 K. (○) DPA; (■) C_6-imine; (◇) propionitrile; (◆) C_6-nitrile; (□) propene; (■) total hydrocarbons; (●) total heavy.

residue builds, but then the residue apparently transforms because the total area increases continuously in the period 11–189 ks.

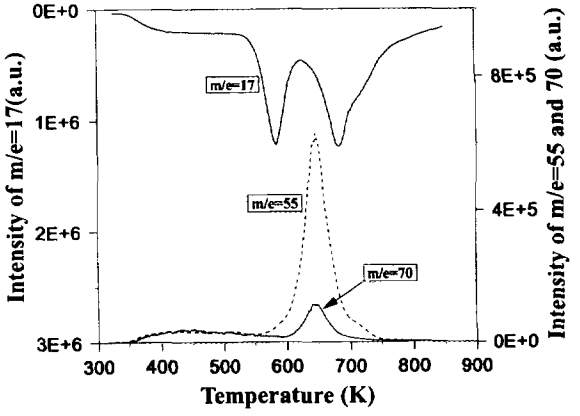

FIG. 16. Ions characteristic of NH_3 (m/e = 17), C_6-nitrile (m/e = 55), and C_6-imine (m/e = 70) during thermal analysis of 1-PA on Cu–MFI.

The enhanced capability of Cu–MFI over Ga–MFI and In–MFI to promote the formation of a long chain nitrile is apparent even at the low 1-PA coverages characteristic of 1-PA thermal analysis in the flow reactor system. Figure 16 shows the appearance of a characteristic peak with $m/$

TABLE 4

Products of the Catalytic Reaction of 1-PA over Cu–MFI at 593 K

Time (ks)	0	1.80	4.08	7.38	11.5	14.7	20.0	30.9	118	189	254
Total peak area	35173	11203	8402	8349	7479	7723	8800	9959	16774	20068	19917
Production distribution											
Hydrocarbons:											
Ethene		59	62	53	73	76	68	73	134	318	355
Ethane										44	34
Propene		86	121	233	220	339	454	592	2163	3579	3965
Propane									209	134	138
Butene-1							122	151	1058	1557	1881
trans-Butene-2							25	39	162	342	518
cis-Butene-2							15	20	105	225	343
3-Methyl-butene-1									56	61	96
Pentene-1				27	26	29	32	25	59	76	101
2-Methyl-butene-1									271	431	562
trans-Pentene-2		114	155	193	203	228	254	360	180	273	388
Pentene-1									32	49	59
cis-Pentene-2		47	66	73	76	94	106	129	96	143	179
2-Methyl-butene-2									728	181	1535
Hexene-1		141	237	388	402	414	483	719	766	762	618
Other hexenes		421	581	810	832	1157	1800	3020	6512	6872	5732
N-containing compounds:											
1-PA		5800	1350	750	300	200	150				
DPA		118	46	102	33	46	20		32		
C_6-Imine		300	402	350	67	115	20				
Propionitrile		872	1460	1515	1482	1506	1597	1594	1630	1083	1507
C_6-Nitrile		2119	2865	3190	3060	2835	3214	3063	2851	2338	1906
Heavier nonidentified:											
26.595[a]		955	953	628	639	613	388	126			
27.946[a]		100	75	37	33	49	52	26			
28.785[a]		71	29		33	22		22			

[a] Retention time (min).

e = 55 during the TA process. This peak is located at 640 K, which is between the two ammonia peaks depicted in Fig. 16. Fragmentation of a C_6-nitrile in the mass spectrometer would be expected to produce m/e = 55 as a more intense ion than m/e = 54, which is an intense fragment of propionitrile. A C_6-imine would be expected to yield m/e = 70 as the most intense ion. Despite some intensity at m/e = 54 (not shown in Fig. 16) and some at m/e = 70 (shown in Fig. 16) in the fragmentation pattern in the same temperature interval, the intensity of the peak for m/e = 55 greatly exceeds that of both other peaks. Therefore, this TA feature can be assigned primarily to desorption of a C_6-nitrile product.

GENERAL DISCUSSION

We originally chose to study the decomposition of 1-PA on MFI for two reasons. First, 1-PA decomposition has been proposed recently as a method for the characterization of Brønsted acidity on zeolites, but whether or not the method is applicable when Lewis acid sites such as metal cations are present in the zeolite has not been discussed. Second, the investigation of the peculiarities of the decomposition of 1-PA adsorbed on MFI may yield a better understanding of the process of template decomposition of "as-synthesized" zeolites. This is a crucial step in obtaining quality adsorbents and catalysts. The results of the present investigation clearly indicate that the replacement of the protons in the MFI zeolite with Ga, In, or Cu cations leads to radical changes in the decomposition reaction of 1-PA. The most important feature that these cations share is the ability to bring together more than one 1-PA molecule at a single site, even at relatively high temperatures. It is this feature which apparently facilitates both the bimolecular transalkylation to DPA and the dehydrogenation processes. In contrast, purely proton forms of MFI do not possess this feature and therefore the unimolecular decomposition to propene and ammonia appears to be the most preferred reaction path unless both excess 1-PA in the gas phase and elevated temperatures are present.

Classic organic chemistry provides a number of analogies between the action of metal ions toward amines in solution and the interaction of propanamine with zeolitic cations. Complexes of cations containing two or more amine molecules are well known (41, 42). Cu^{2+}/Y is an example of a metal cation-containing zeolite which is known to multiply coordinate amines in well-defined complexes (43). Moreover, the condensation reactions of carbonyl compounds with primary amines are influenced by the presence of metal ions in solution. For example, the condensation of methylamine with α-diketones in the presence of a metal ion results in imine formation, while in the absence of a metal ion diimines and polymeric condensation products are formed (42).

The conversion of alkylamines on alumina has been intensively studied and the formation of both *N*-alkylidenalkylamines and corresponding alkanenitriles have been discussed in terms of the cooperative action of acidic and basic centers on the surface of alumina catalysts (31, 32). It was postulated that the dehydrogenation reactions were catalyzed by Lewis acid sites (31); however, the primary reaction of alkylamines catalyzed by alumina is deammination. In contrast, we observe that transalkylation and dehydrogenation represent the primary reactions of 1-PA catalyzed by a reduced Ga–MFI catalyst, at a temperature as low as 593 K. Along with previously observed products of 1-PA conversion on alumina such as DPA, C_6-imine, and propionitrile, we observe a C_6-nitrile (2-methlypentanenitrile) which has never before been mentioned as a product of 1-PA conversion. Additional investigations are necessary to elucidate the mechanism of this reaction. We think that the appearance of this product is closely related to the reactivity of the alpha carbon of the nitriles or the beta carbon of the imine. It is also possible that a reaction similar to a Stevens rearrangement (e.g., (41)) of an adsorbed C_6-imine or DPA can account for the formation of a nitrile with a longer alkyl chain than that of the starting reagent.

The nature of the zeolite metal ion plays an important role in the interactions between ion, 1-PA, and some products of the initial propanamine transformations. The catalytic data obtained here show that the extent of the dehydrogenation reactions differs depending on the nature of the cation. The C_6-imine appears as a primary product of 1-PA conversion catalyzed by In–MFI, while Ga–MFI and Cu–MFI catalyze the production of more dehydrogenated products such as propionitrile and a C_6-nitrile, respectively. It is difficult to determine the exact mechanism of 1-PA transformations on cation-containing zeolites because the different reaction pathways of transalkylation, dehydrogenation, deammination, oligomerization, and possibly others contribute to a very complicated reaction network. Furthermore, the possible reactions of propanamine are certainly not restricted to reactions [2]–[13]. It cannot be excluded, for example, that the formation of reactive propylimine according to reactions [14] and [15] plays a crucial role in a cyclic-type mechanism for propanamine conversion similar to that proposed in the alumina-catalyzed transformation of amines (32) and the copper-catalyzed dehydroamination of alcohols (22).

$$C_3H_7NH_2 \rightarrow C_3H_6NH + H_2 \qquad [14]$$

$$2C_3H_7NH_2 \rightarrow C_3H_6NH + C_3H_6 + NH_3 + H_2. \qquad [15]$$

However, a simplified comparison of the isothermal reaction results (Figs. 11, 13, and 15) reveals certain trends. If we use only the data at short times (therefore

more characteristic of the primary reactions), we can approximate the overall bimolecular transalkylation activity of a catalyst as

$$\theta = (\text{area DPA}) + (\text{area } C_6\text{-imine}) + (\text{area } C_6\text{-nitrile}), \quad [16]$$

and using the stoichiometry of the dehydrogenation reactions [9]–[13] we can approximate the overall dehydrogenation activity as

$$\eta = (2)(\text{area } C_3\text{-nitrile}) + (2)(\text{area } C_6\text{-nitrile}) + (\text{area } C_6\text{-imine}). \quad [17]$$

By these measures the relative activities of the cation-containing zeolites are

$$\theta_{Ga} \gg \theta_{In} \gg \theta_{Cu} \quad [18]$$

$$\eta_{Cu} \gg \eta_{Ga} > \eta_{In}. \quad [19]$$

The θ-scale probably reflects the Lewis acidity of the cations within the zeolite. The electron-withdrawing nature of the zeolite lattice generates stronger Lewis acidity of the cation. For Ga this can be measured by changes in EPR intensity upon adsorption of electron donors (44), or in the IR frequency of pyridine adsorption (45) or of CO adsorption (46). On the latter scale, Ga^{3+} and Al^{3+} are of roughly equal strength. In^{3+} and Cu^{2+}, with smaller charge/radius ratios, should be weaker, because the strength of the Lewis acids tested in bonding to CO followed this trend well. We should note here that, although the reduced forms of these cations are those typically observed in the presence of H_2 at high temperature (34, 37, 47, 48), the recombinative dissociation of H_2 in the dehydrogenation reactions requires that the cation be present in both its oxidized and reduced forms during catalysis.

Measurements of NH_3 heats of adsorption at zero coverage for several series of oxides confirm that Ga^{3+} is a strong Lewis acid; in fact, Ga_2O_3 is by this measurement a stronger Lewis acid than all the transition metal oxides and at least as strong as any of the amphoteric oxides of the posttransition metals (49).

The η-scale probably reflects the reducibility of the cations, In^{3+} being most reducible. Within zeolite crystals, Cu^{2+} is typically very stable, being regenerated at relatively low temperatures in the presence of oxidizing agents (50). Therefore, it is not surprising that Cu was the best cation for promoting dehydrogenation, because the desorption of H_2, with oxidation of the cation, appears to be the rate-limiting step in most of the hydrocarbon dehydrogenation reactions catalyzed by metal-exchanged zeolites (36).

In conclusion, there appears to be tremendous potential for cation-containing zeolites in catalyzing specific and sometimes unexpected transformations with amines. Further investigations are still necessary to elucidate the extent to which this potential can be utilized in the steadily growing field of organic synthesis using zeolite catalysts.

ACKNOWLEDGMENTS

The authors gratefully acknowledge the financial support of the Department of Energy (Grant DE-FG05-92ER14291) and the Exxon Education Foundation.

REFERENCES

1. Barrer, R. M., "Hydrothermal Chemistry of Zeolites," Academic Press, New York, 1982.
2. Breck, D. W., "Zeolite Molecular Sieves," Wiley, New York, 1974.
3. Szostak, R., "Molecular Sieves: Principles of Synthesis and Identification," Van Nostrand–Reinhold, New York, 1988.
4. Rabo, J. H. (Ed.), "Zeolite Chemistry and Catalysis," ACS monograph 171. American Chemical Society, Washington, DC, 1976.
5. Occelli, M. L., and Robson, H. E. (Eds), "Zeolite Synthesis," ACS monograph 398. American Chemical Society, Washington, DC, 1989.
6. Wu, E. L., Whyte, T. E., Jr., and Venuto, P. B., *J. Catal.* **21,** 384 (1971).
7. Wu, L. L., Kuhl, G. H., Whyte, T. E., Jr., and Venuto, P. B., *Adv. Chem. Ser.* **101,** 490 (1971).
8. Jacobs, P. A., and Uytterhoeven, J. B., *J. Catal.* **26,** 175 (1972).
9. Fripiat, J. J., and Lambert-Nelsen, M. M., *Adv. Chem Ser.* **124,** 518 (1973).
10. Parker, L. M., Bibby, D. M., and Patterson, J. E., *Zeolites* **4,** 168 (1984).
11. Bilger, S., Soulard, M., Kessler, H., and Guth, J. L. *Zeolites* **11**(8), 784 (1991).
12. Soulard, S., Bilger, S., Kessler, H., and Guth, J. L., *Thermochim. Acta* **204,** 167 (1992).
13. Bourgeat-Lami, E., Renzo, F. D., Fajula, F., Mutin, D. H., and Courieres, T. D., *J. Phys. Chem.* **96**(9), 3807 (1992).
14. Gricus Kofke, T. J., Gorte, R. J., and Farneth, W. E., *J. Catal.* **114,** 34 (1988).
15. Gricus Kofke, T. J., Gorte, R. J., and Kokotailo, G. T., *Appl. Catal.* **54,** 177 (1989).
16. Gricus Kofke, T. J., Gorte, R. J., and Kokotailo, G. T., *J. Catal.* **116,** 252 (1989).
17. Parrillo, D. J., Adams, A. T., Kokotailo, G. T., and Gorte, R. J., *Appl. Catal.* **67,** 197 (1990).
18. Parrillo, D. J., Dolenec, D., Gorte, R. J., and McCabe, R. W., *J. Catal.* **142,** 708 (1993).
19. Hurd, C. D., and Carnaham, F. L., *J. Am. Chem. Soc.* **52,** 4151 (1930).
20. Sabatier, P., and Gandion, E., *Compt. Rend.* **165,** 224 (1917).
21. Upson, F. W., and Sands, L., *J. Am. Chem. Soc.* **45,** 2306 (1922).
22. Baiker, A., and Kijenski, J., *Catal. Rev.—Sci. Eng.* **27**(4), 653 (1985).
23. Taylor, A., *J. Phys. Chem.* **34,** 2761 (1930).
24. Taylor, A., *J. Phys. Chem.* **36,** 670 (1932).
25. Taylor, A., and Achilles, H. E., *J. Phys. Chem.* **35,** 2658 (1931).
26. Xu, B. Q., Yamaguchi, T., and Tanabe, K., *Chem. Lett.*, 281 (1988).
27. Xu, B. Q., Yamaguchi, T., and Tanabe, K., *Chem. Lett.*, 149 (1989).
28. Kanazirev, V., Dooley, K. M., and Price, G. L., *J. Catal.* **146,** 228 (1994).

29. Park, Y. H., and Price, G. L., *Ind. Eng. Chem. Res.* **30,** 1700 (1991).
30. Shyr, Y. N., and Price, G. L., *Ind. Eng. Chem. Prod. Res. Dev.* **23,** 536 (1984).
31. Brey, W. S., and Cobbledic, D. S., *Ind. Eng. Chem.* **51,** 103 (1959).
32. Sedlacek, J., and Koubek, J., *Collect. Czech. Chem. Commun.* **48,** 755 (1983).
33. Kanazirev, V., Price, G. L., and Dooley, K. M., *Catal. Lett.*, **24,** 227 (1994).
34. Price, G. L., and Kanazirev, V., *J. Catal.* **126,** 267 (1990).
35. Price, G. L., and Kanazirev, V., *J. Mol Catal.* **66,** 115 (1991).
36. Iglesia, E., Baumgartner, J. E., and Price, G. L., *J. Catal.* **134,** 549 (1992).
37. Meitzner, G. D., Iglesia, E., Baumgartner, V. E., and Huang, E. S., *J. Catal.* **140,** 209 (1993).
38. Meriaudeau, P., and Naccache, C., *in* "Zeolite Chemistry and Catalysis" (P. A. Jacobs, N. I. Jaeger, L. Kubelkova, and B. Wichterlova, Eds.), p. 405. Elsevier, Amsterdam, 1991.
39. Kanazirev, V., Neinska, Y., Tsoncheva, T., and Kosova, L., *in* "Proceedings, 9th International Zeolite Conference, Montreal, 1992" (R. von Ballmoos, J. B. Higgins, and M. J. J. Treacy, Eds.), Vol. 1, p. 461. Butterworths, London, 1993.
40. Karge, H. G., Wichterlova, B., and Beyer, H. K., *J. Chem. Soc., Faraday Trans.*, **88**(9), 1345 (1992).
41. Smith, J. W., *in* "The Chemistry of the Amino Group" (S. Patai, Ed.), p. 195. Interscience, London/New York/Sydney, 1968.
42. Sollenberger, P. Y., and Martin, R. B., *in* "The Chemistry of the Amino Group" (S. Patai, Ed.), p. 355. Interscience, London/New York/Sydney, 1968.
43. Peigneur, P., Lunsford, J. H., Wilde, W., and Schoonheydt, R. A., *J. Phys. Chem.* **81,** 1179 (1977).
44. Khodakov, A. Yu., Kustov, L. M., Bondarenko, T. N., Dergachev, A. A., Kazansky, V. B., Minachev, Kh. M., Borbely, G., and Beyer, H. K., *Zeolites* **10,** 603 (1990).
45. Roessner, F., Hagen, A., Mroczek, U., Karge, H. G., and Steinberg, K.-H., *in* "Proceedings, 10th International Congress on Catalysis Budapest," Vol. B, p. 1707. 1993.
46. Rommanikov, V. N., Paukshtis, E. A., and Ione, K. G., *in* "Chemistry of Microporous Crystals" (T. Inui, S. Namba, and T. Tatsumi, Eds.) p. 311. Elsevier, Amsterdam, 1991.
47. Kanazirev, V., Price, G. L., and Dooley, K. M., *in* "Zeolite Chemistry and Catalysis" (P. A. Jacobs, N. I. Jaeger, L. Kubelkova, and B. Wichterlova, Eds.), p. 277. Elsevier, Amsterdam, 1991.
48. Carli, R., Bianchi, C. L., Giamantonio, R., and Ragaini, V., *J. Mol. Catal.* **83,** 379 (1993).
49. Auroux, A., and Gervasini, A., *J. Phys. Chem.* **94,** 6371 (1990).
50. Petunchi, J. O., and Hall, W. K., *J. Catal.* **80,** 403 (1983).